



Mild and controllable solid electrolyte interphase formation for high-voltage lithium metal batteries in a wide-temperature range from $-40\text{ }^{\circ}\text{C}$ to $80\text{ }^{\circ}\text{C}$

Jialin Li^a, Haiming Hua^a, Xiaodie Deng^a, Pengbin Lai^a, Yuanhong Kang^a, Silan Kuang^a, Fei Wang^a, Xiaoyuan Zeng^{b,*}, Yingjie Zhang^b, Jinbao Zhao^{a,*}

^a College of Chemistry and Chemical Engineering, State-Province Joint Engineering Laboratory of Power Source Technology for New Energy Vehicle, State Key Laboratory of Physical Chemistry of Solid Surfaces, Engineering Research Center of Electrochemical Technology, Ministry of Education, Collaborative Innovation Center of Chemistry for Energy Materials, Xiamen University, Xiamen 361005, China

^b National and Local Joint Engineering Laboratory for Lithium-ion Batteries and Materials Preparation Technology, Key Laboratory of Advanced Battery Materials of Yunnan Province, Faculty of Metallurgical and Energy Engineering, Kunming University of Science and Technology, Kunming 650093, China

ARTICLE INFO

Keywords:

Solvation structure
Diluent
High-voltage
Wide-temperature
Lithium metal full-cells

ABSTRACT

Wide-temperature and high-voltage lithium metal batteries (LMBs) have great potential in electric vehicles, but their applications face major challenges due to unstable interfacial layers. Here, a dual-salt (lithium bis(trifluoromethanesulfonyl) and lithium difluoro(oxalato)borate) ether-based localized high-concentration electrolyte (LHCE) is designed to facilitate the formation of salt-derived interfacial layers. It is proved that the presence of diluent makes the formation of solid electrolyte interphase (SEI) mild and controllable, thereby avoiding the overproduction of reduction product and improving the reversibility of lithium metal anode. Therefore, the electrolyte achieves a high average Coulombic efficiency (CE) of 99.5 % for Li||Cu cell and stable cycling of 4.5 V Li||LiNi_{0.5}Co_{0.2}Mn_{0.3}O₂ (NCM523) cell. Benefiting from the excellent compatibility of electrolyte with electrodes, the Li||NCM523 full-cell provides excellent cycling stability under severe conditions (4.5 V, negative/positive capacity ratio \approx 0.9). Furthermore, the electrolyte exhibits excellent wide-temperature electrochemical performance, enabling the cells to provide 71 % of room-temperature capacity at $-40\text{ }^{\circ}\text{C}$ and retain 85 % capacity retention after 200 cycles with high CE at $80\text{ }^{\circ}\text{C}$. This study shares a new insight into the role of diluent and provides a promising strategy for electrolyte design of wide-temperature and high-voltage LMBs.

1. Introduction

With the development of the electric vehicles and other industries, the demand for lithium batteries with high energy density suitable for a wide-temperature range is growing rapidly [1–5]. Lithium metal anode (LMA) is considered to be the most ideal anode due to its high theoretical specific capacity (3860 mAh/g) and the lowest standard electrode potential (-3.04 V versus the standard hydrogen electrode), which can effectively improve the energy density of batteries and has attracted extensive attention from researchers [6–8]. Although the research on lithium metal batteries (LMBs) began half a century ago, the problems of lithium dendrites growth and interfacial instability during the lithium deposition/stripping process have not been completely solved, which have prevented LMBs from being practically applied so far [6].

Among various strategies to improve the electrochemical performance of LMBs, electrolyte engineering is considered as a simple and practical approach [8,9]. Considering the inherent thermodynamic instability [10] and the huge volume change during cycling of LMA, an ideal electrolyte for LMBs should be able to grow uniform SEI with high mechanical strength and stability in situ on LMA, so as to inhibit lithium dendrite growth and improve the cycle stability [11]. Unfortunately, the carbonate electrolytes commonly used in lithium-ion batteries are not suitable for LMBs and inevitably form unstable SEI and lithium dendrites [12,13]. Compared with other non-aqueous electrolytes, ether-based electrolytes are more suitable for LMBs due to their advantage of higher reduction stability [14,15]. On the other hand, the compatibility of electrolyte with high-voltage cathode is also crucial for the development of high-energy-density LMBs [16]. Nevertheless, ether-based

* Corresponding authors.

E-mail addresses: zengxiaoyuan721@126.com (X. Zeng), jbzhao@xmu.edu.cn (J. Zhao).

<https://doi.org/10.1016/j.cej.2022.139398>

Received 9 August 2022; Received in revised form 19 September 2022; Accepted 20 September 2022

Available online 23 September 2022

1385-8947/© 2022 Elsevier B.V. All rights reserved.

electrolytes with conventional concentration (1 M) have poor oxidative stability and can only be adapted to cathode materials below 4 V, such as LiFePO₄ [17,18].

In order to enhance the compatibility of electrolyte with electrodes, some researchers have focused their research on high-concentration electrolytes (HCEs) [16,19–22] and localized high-concentration electrolytes (LHCEs) [13,23–27] from the perspective of solvation structure [28]. In HCE, most solvent molecules are coordinated with Li⁺ and free solvent molecules are greatly reduced, effectively suppressing their decomposition at the cathode, which improves the oxidative stability of the electrolyte and broadens its application in high-voltage batteries. Besides, more anions enter the solvation layer of Li⁺ to form contacting ion pair (CIP) and cation-anion aggregate (AGG). Such solvated complexes promote the formation of salt-derived, inorganic-rich interfacial layer with higher ionic conductivity and mechanical strength [21,29]. Since a good interfacial layer depends to a considerable extent on the decomposition of anions, the choice of lithium salt plays an important role in the composition and structure of the interfacial layer [30]. LHCE is obtained by adding diluent (such as 1,1,2,2-tetrafluoroethyl-2,2,3,3-tetrafluoropropylether, TTE [31–33]) to HCE, and its viscosity and cost are obviously reduced while retaining the solvation structure of HCE. In addition, there is evidence that LMA is more reversible in LHCE than in HCE [26,34]. Although there is a correlation between the solvation structure of the electrolyte and the composition and structure of the SEI, the difference in electrochemical performance between LHCE and HCE with similar solvation structure cannot be explained in this way. Therefore, the effect of diluent needs to be further explored.

In our work, it is demonstrated that the diluent TTE slows the formation rate of salt-derived SEI by reducing the concentration of solvated complexes. A dual-salt ether-based LHCE with lithium bis(trifluoromethanesulfonyl) (LiTFSI) and lithium difluoro(oxalato)borate (LiDFOB) (LHCE-LiTD55) is designed, and the mild and controllable SEI formation enables LHCE-LiTD55 to exhibit excellent LMA compatibility. At a current density of 0.5 mA cm⁻², the average Coulombic efficiency (CE) of Li||Cu cells is 99.5 %, which is significantly higher than that of HCEs with similar solvated structures but without TTE. In addition, LHCE-LiTD55 exhibits high oxidation stability, achieving stable cycling of Li||LiNi_{0.5}Co_{0.2}Mn_{0.3}O₂ (NCM523) cell at a high cut-off voltage of 4.5 V, with a capacity retention of 90 % after 200 cycles. Benefiting from the high lithium reversibility and high oxidation resistance of LHCE-LiTD55, the Li||NCM523 full-cell with limited lithium (0.9 × excess) maintains 70 % of the capacity for 175 cycles at a cut-off voltage of 4.5 V. Not only that, LHCE-LiTD55 shows excellent low-temperature (−40 °C) discharge performance and high-temperature (80 °C) cycling stability. Due to the advantages in performance and the interpretation of the effect of diluent, this work provides a reference for the design of electrolytes for wide-temperature and high-voltage LMBS.

2. Experimental section

2.1. Materials preparation

LiNi_{0.5}Co_{0.2}Mn_{0.3}O₂ (NCM523) cathode material was provided by Beijing Easpring Material Technology Co., Ltd. LiTFSI and LiDFOB were provided by Zhangjiagang Guotai Huarong New Chemical Materials Co., Ltd. 1,2-dimethoxyethane (DME) and TTE were purchased from Energy Chemical and Beijing Hwrk Chemicals Limited, respectively. Lithium sheets (16 mm diameter, 1 mm thick) were purchased from China Energy Lithium Co., Ltd. LB-301 (1 mol/L LiPF₆ in EC/DMC, 1:1 by wt.) was provided by Zhangjiagang Guotai Huarong New Chemical Materials Co., Ltd. The LHCEs were prepared by mixing LiTFSI, LiDFOB, DME and TTE according to n_{LiTFSI}:n_{LiDFOB}:n_{DME}:n_{TTE} = 1:0:1.8:3, 0.5:0.5:1.8:3, 0.3:0.7:2:3, 0:1:2:3 to obtain LHCE-LiTFSI, LHCE-LiTD73, LHCE-LiTD55, LHCE-LiTD37, LHCE-LiDFOB. The dual-salt HCE (HCE-LiTD55) and dual-salt dilute electrolyte (DE-LiTD55) were prepared by mixing LiTFSI, LiDFOB, DME and TTE according to n_{LiTFSI}:n_{LiDFOB}:n_{DME}

= 0.5:0.5:1.8, 0.5:0.5:9.

For the preparation of the low-loading cathode and the high-loading cathode, NCM523, acetylene black (AB) and poly(vinylidene fluoride) (PVDF) were mixed at mass ratios of 8:1:1 and 94:3:3, respectively. *N*-methyl-2-pyrrolidone (NMP) solvent was added to the mixture to adjust to the proper viscosity. After that, the slurry was stirred for 6 h (h), then coated on Al foil and dried under vacuum at 80 °C for 12 h to remove NMP. The cathodes were punched into circular pieces with a diameter of 12 mm. The mass loadings of the active cathode material in the low-loading cathode and high-loading cathode are about 3 mg cm⁻² and 13 mg cm⁻², respectively.

2.2. Physical properties measurement

A conductivity meter (DDS-307A, Leici) and a conductivity electrode (DJS-1C, Leici) were used to measure the ionic conductivity of electrolytes. The viscometer (VM-10A-L, Sekonic Cooperation) was applied to measure the viscosity of the electrolytes. The contact angles between the electrolytes and the separator were obtained using the contact angle tester (JC-2000C1). ⁷Li NMR spectra were acquired by the AVANCE NEO 500 MHz Digital FT NMR Spectrometer and a capillary tube filled with 0.1 M LiClO₄ in D₂O was used to lock the field. Raman spectra were acquired on the confocal in situ Raman spectroscopy (LabRAM HR Evolution). The surface morphology of Lithium was observed by a field emission scanning electron microscope (Zeiss Gemini SEM 500) operated at 1.0 kV. The surface morphology of the cycled cathode was photographed by scanning electron microscope (SEM, Hitachi TM3030). X-ray diffraction (XRD) spectra were tested on Rigaku Miniflex 600 X-ray diffractometer. The cathode used for SEM and XRD tests was disassembled from Li||NCM523 cell after 200 cycles between 3.0 and 4.5 V. The components of SEI and cathode electrolyte interface (CEI) was analyzed by Thermo Fisher ESCALAB Xi + X-ray photoelectron spectroscopy (XPS). Lithium sheets used to test the components of the SEI were disassembled from Li||Li symmetric cells after 10 cycles. The etching rate of SEI is 0.2 nm s⁻¹ (calculated by the etching rate of Ta₂O₅). The cathodes used to test the components of CEI were disassembled from Li||NCM523 cells after 10 cycles between 3.0 and 4.5 V. Differential scanning calorimetry (DSC) was tested using a STA 449 F3 Jupiter. The NCM523 cathode was charged to 4.3 V, then disassembled and rinsed with DME to remove residual solvent and lithium salts. Then take 3 mg of charged cathode material and 3 μL of LHCE-LiTD55 for DSC test. DSC tests were also performed on LHCE-LiTD55 alone. The heating rate in DSC tests is 5 °C min⁻¹.

2.3. Electrochemical characterization

The Li||Li symmetrical cells were 2032-type coin cells and other cells were 2016-type coin cells. All types of cells were added 75 μL of electrolyte and assembled in glove box (Braun) filled with argon. Celgard2500 separator was used to assemble the cells. The cells would be left for 10 h before testing the electrochemical characterization. The Li||Li symmetrical cell, which was used for long-cycle test (0.5 mA cm⁻², 1.0 mAh cm⁻²), consisted of two lithium sheets with a diameter of 16 mm and a piece of separator. The Li||Al cells, with lithium sheet (12 mm diameter) as the working electrode and aluminum foil (16 mm diameter) as the counter electrode, were used for linear sweep voltammetry (LSV) and chronoamperometry (CA) test. LSV was conducted by sweeping the voltage (0.1 mV s⁻¹) of Li||Al cells from the open circuit voltage to 5.5 V. The CA test is to keep the Li||Al cells at a constant voltage of 4.5 V for 5 h. Li||Cu cells were applied to CV tests, the average CE tests and lithium deposition morphology tests, using Cu foil (16 mm diameter) and lithium sheet (12 mm diameter) as working electrode and counter electrode, respectively. CV curves were tested by assembling Li||Cu cells and scanning between 0 and 3 V. LSV, CA and CV tests were performed on the electrochemical workstation (CHI660E). The average CEs of lithium deposition/stripping process were tested using the method 3

[35]. The first step was a pretreatment, depositing 5.0 mA h cm^{-2} lithium on the Cu foil, and then charging the Li||Cu cells to 1 V. The next step was to deposit 5.0 mA h cm^{-2} (Q_T) lithium on the Cu foil, and then cycle 100 times (n) with 1.0 mA h cm^{-2} (Q_C). Finally, the Li||Cu cells were charged to 1 V to strip all the Li metal on the Cu foil (Q_S). The formula for calculating the average CE is as follows:

$$CE = \frac{Q_S + nQ_C}{Q_T + nQ_C} \quad (1)$$

The Li||NCM523 cells, used for long-cycle tests at room temperature and high temperature (60°C and 80°C), and low temperature (-40°C) discharge tests, were assembled with the low-mass loading cathodes, separators, and lithium sheets (16 mm diameter). Before the low temperature discharge test, the cell was charged and discharged twice at 0.1 C and then charged to 4.5 V at 0.1 C at room temperature. Put the cell in the refrigerator at -40°C for two hours, then discharge it to 3.0 V at 0.1 C. For the long-cycle stability test, the cells were first charged and discharged at 0.1 C for one cycle, and then cycled at a rate of 1 C (1 C = 160 mAh/g for 4.3 V, 1 C = 180 mAh/g for 4.5 V). For the rate performance test, the charge rate was always 0.1 C, and the discharge rate was changed every 5 cycles. For the assembly of the lithium metal full-cells, the Li@Cu electrodes were prepared by depositing precalculated lithium on the pretreated copper foil and disassembled from the Li||Cu cells. The pretreatment of Cu foil was the same as the tests of the average CEs of Li||Cu cells. Then the high-loading cathode, separator and the Li@Cu

electrode were sandwiched together to assemble lithium full-cell. The Li||NCM523 full-cells were charged and discharged at a current density of 0.1 mA cm^{-2} for the initial cycle. Then full-cells were charged at a current density of 0.5 mA cm^{-2} and discharged at a current density of 1.5 mA cm^{-2} for the long-term cycle. The actual N/P of lithium metal full-cells was referenced to Qiu's method [36], which is measured by assembling Li@Cu||Cu cells and then charging to 1 V.

3. Results and discussion

3.1. Physical and chemical properties of electrolytes

The ionic conductivity and viscosity of different electrolytes are shown in Fig. S1. The conductivity of LHCEs (LHCE-LiTFSI, LHCE-LiTd55, LHCE-LiDFOB) and dual-salt HCE (HCE-LiTd55) is lower than that of dual-salt dilute electrolyte (DE-LiTd55), indicating the dissociation of lithium salts is incomplete in LHCE and HCE. Compared with HCE-LiTd55, the viscosity and contact angle (Fig. S2) of LHCE-LiTd55 decrease significantly, indicating that the addition of diluent TTE effectively improves the viscosity and wettability of the electrolyte.

The oxidative stability of electrolyte determines its compatibility with high-voltage cathode, and the results of LSV test show that the oxidation potential is greatly affected by the solvation structure and the type of lithium salt (Fig. 1a). The oxidation potential of LHCE-LiTd55 is higher than 4.5 V, which is significantly higher than that of DE-LiTd55

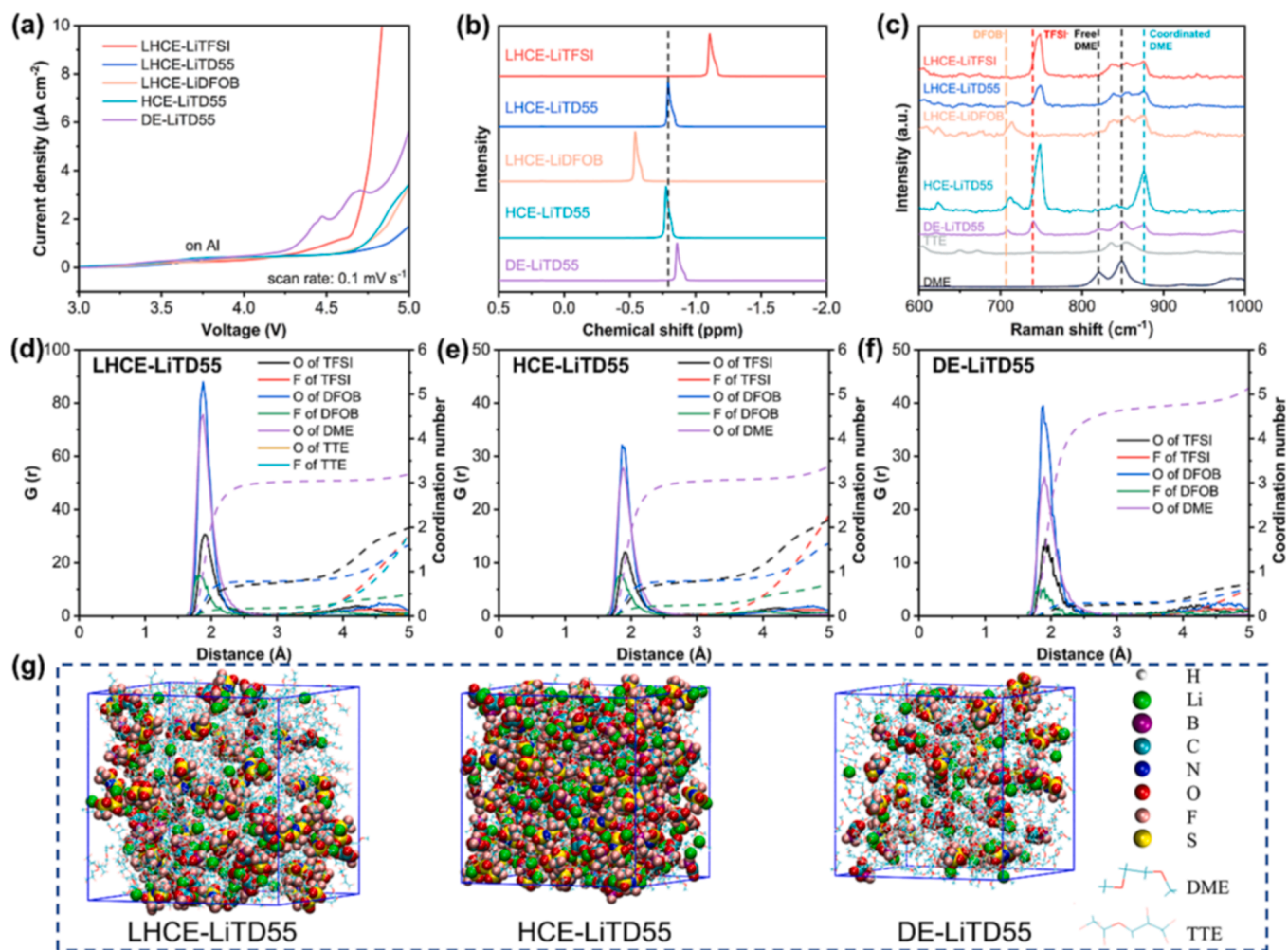


Fig. 1. (a) LSV results of Li||Al cells in different electrolytes at a scan rate of 0.1 mV s^{-1} . (b) ^7Li NMR spectra and (c) Raman spectra of different electrolytes. Radial distribution function and coordinated number of (d) LHCE-LiTd55, (e) HCE-LiTd55 and (f) DE-LiTd55. (g) MD simulation snapshots of LHCE-LiTd55, HCE-LiTd55 and DE-LiTd55.

(4.2 V). The broadened electrochemical window of LHCE-LiTD55 is mainly due to fewer free DME molecules, which will be demonstrated by the following characterizations. In addition, the oxidation current of LHCE-LiTD55 at high voltage is lower than that of HCE-LiTD55 due to the lower HOMO level of TTE (Fig. S3). However, the oxidation current of LHCE-LiTFSI increases around 4.3 V, which is significantly lower than that of other LHCEs. To explore the reason for the narrow electrochemical window of LHCE-LiTFSI, CA test was carried out to test the current response versus time by applying a voltage of 4.5 V on the Li||Al cells with different electrolyte (Fig. S4). The current of Li||Al cell in LHCE-LiTFSI first decreases and then increases rapidly, which is opposite to the trend of LHCE-LiTD55 and LHCE-LiDFOB. The Li||Al cells were disassembled after the CA test to obtain Al foil and separator. Optical photographs (Fig. S5a–c) and SEM images (Fig. S5d–i) show that severe side reaction occurs and cracks appear on the surface of the Al foil in LHCE-LiTFSI, while no obvious corrosion occurs in LHCE-LiTD55 and LHCE-LiDFOB. Therefore, TFSI⁻ in LHCE can also severely corrode the Al current collector at high voltage, thus increasing its specific surface area and causing more severe corrosion. By replacing part of TFSI⁻ anions with DFOB⁻, the corrosion of Al current collector can be effectively inhibited.

The solvation structure of the electrolyte affects its physical and electrochemical properties. The chemical shifts of the ⁷Li NMR peaks vary greatly due to changes in the solvation structure. The ⁷Li NMR spectra of different electrolytes are shown in Fig. 1b. The chemical shift is greatly affected by the type of anion. The chemical shift of LHCE-LiDFOB is the largest, followed by LHCE-LiTD55, and LHCE-LiTFSI is the smallest, indicating that TFSI⁻ coordinates Li⁺ to enhance the shielding effect, while DFOB⁻ coordinates Li⁺ to weaken the shielding effect. The chemical shift of HCE-LiTD55 is lower than that of DE-LiTD55, suggesting that increasing the concentration of lithium salt changes the coordination environment of Li⁺. The similar chemical shifts of LHCE-LiTD55 and HCE-LiTD55 indicate that the addition of TTE does not change the solvation structure of the electrolyte. The comparison of Raman spectra of different electrolytes (Fig. 1c, Fig. S6) further confirms the difference in solvation structure among LHCE, HCE and DE. The spectral peaks corresponding to the S–N stretching vibration of TFSI⁻ [37,38] and the ring breathing vibration of DFOB⁻ [39] are sensitive to the coordination of Li⁺, and shift to higher wave numbers in LHCEs and HCE-LiTD55 compared to DE-LiTD55, which indicates that TFSI⁻ and DFOB⁻ are more involved in the coordination of Li⁺ in LHCEs and HCE to form CIP and AGG solvated complexes. The 820 and 850 cm⁻¹ characteristic peaks attributed to C–O–C stretching and CH₂ rocking modes of free DME molecule [40] are obvious in the Raman spectrum of DE-LiTD55, but significantly decrease in the Raman spectrum of LHCEs and HCE-LiTD55, and are replaced by new peak near 875 cm⁻¹, corresponding to Li⁺-coordinated DME. This result indicates that free DME molecules in LHCEs and HCE are considerably reduced, which is beneficial to the increase of oxidative stability.

Molecular dynamics (MD) simulation was also conducted to simulate the solvation structure of different electrolytes (Fig. 1d–g, Fig. S7). In DE-LiTD55, Li⁺ is mainly coordinated by DME, which has an average coordination number of 4.26 DME oxygens per Li⁺. When the ratio of lithium salt to DME is increased, the coordination number of DME in LHCEs and HCE-LiTD55 is significantly reduced, accompanied by an increase in the coordination number of anions (Table S2). The solvation structure consists mainly of CIP and AGG. The proportion of free DME molecules in LHCE-LiTD55 is similar to that of HCE-LiTD55 and significantly smaller than that of DE-LiTD55 (Table S6). What's more, the coordination number of TTE in LHCE-LiTD55 is close to 0, and the coordination number of LHCE-LiTD55 is almost the same as that of HCE-LiTD55, indicating that TTE hardly change the solvation structure (Table S2). The results of MD simulation are consistent with NMR and Raman spectroscopy. But the presence of TTE in LHCE-LiTD55 partially breaks the Li⁺-coordinated cross-linked network (Fig. 1g), and reduces the concentration of solvated complexes and free DME molecules

compared to that in HCE-LiTD55, and its impact on electrochemical performance will be discussed further.

3.2. Reversibility of LMA deposition/stripping process

In order to verify the reversibility of LMA deposition/stripping process, the average CEs of Li||Cu cells in above electrolytes were tested using method 3 reported by Adams et al. [35] Apparent differences in average CEs can be observed in different LHCEs and higher average CEs of Li||Cu cells are obtained in dual-salt LHCEs (Fig. 2a, b, Fig. S8). Especially when the ratio of the two lithium salts is 1:1, the average CE of Li||Cu cell in LHCE-LiTD55 reaches 99.5 %, which is close to the best results reported (Table S8). For comparison, the average CEs of LHCE-LiTFSI and LHCE-LiDFOB are 96.8 % and 99.0 %, respectively, lower than that of LHCE-LiTD55. This demonstrates the effectiveness of the synergistic effect of LiTFSI and LiDFOB. On the other hand, although the solvation structures of the two electrolytes are almost identical, the CE of HCE-LiTD55 is significantly lower than that of LHCE-LiTD55, indicating that the solvation structure is not the only factor affecting the reversibility of LMA. In addition, Li||Cu cells in DE-LiTD55 and LB-301 could not complete the test of average CE, which is due to their instability to lithium (Fig. 2c).

The cycling performance of the Li||Li symmetric cells (Fig. 2d, Fig. S9) further confirms the role of the synergistic effect of the dual-salt and the presence of TTE in improving the reversibility of LMA. Li||Li symmetric cell maintains lower polarization voltage over longer cycle time in LHCE-LiTD55 than in other electrolytes. In contrast, although the cell using HCE-LiTD55 can cycle stably for about 1000 h, its polarization voltage is about twice that of LHCE-LiTD55. The impedances of Li||Li symmetrical cells at different cycle time were also tested and compared (Fig. S10). The impedance of the cell in LHCE-LiTD55 is consistently lowest after 200 h, which is consistent with its overpotential.

In order to explore the deposition behavior of lithium in different electrolytes, 5 mAh cm⁻² lithium was deposited on the copper foil at a current density of 0.5 mA cm⁻², and the morphology of the surface was photographed (Fig. 3a, Fig. S11). Large and dense lithium is deposited in LHCE-LiTD55 without dendrites. Lithium deposited in HCE-LiTD55 is also large, but less dense. However, in DE-LiTD55, and LB-301, the deposited lithium presents a porous, dendritic growth morphology. The above results show that designing from the type of lithium salt and solvation structure can improve the morphology of deposited lithium and avoid the growth of dendrites.

Since SEI affects the reversibility of LMA, XPS test was performed on the surface of LMA after cycling (Fig. 3b, Fig. S12). According to the C 1s spectrum, the content of C species in the SEI formed by LB-301 is significantly higher than that formed by other electrolytes, which indicates a serious side reaction between carbonate electrolyte and LMA. There is much C-F in the SEI formed by LHCE-LiTFSI and DE-LiTD55, indicating that there are a lot of primary decomposition products of LiTFSI on the surface of LMA. For LHCE-LiTD55 and HCE-LiTD55, the content of each component of the formed SEI is very similar, which indicates that TTE has little contribution to the components. Due to the addition of LiDFOB, a large amount of B species and polyether appear in SEI formed by LHCE-LiTD55 and HCE-LiTD55, which helps to improve the flexibility of the SEI [26]. Interestingly, although TFSI⁻ is also decomposed at the surface as can be seen from the N 1s and S 2p spectra, C-F is barely visible in the C 1s and F 1s spectra. This may be due to the synergistic effect of LiDFOB and LiTFSI, so that TFSI⁻ is more completely reduced, and more favorable species such as LiF, Li₃N, and Li_xN_oy are generated. LiF has the characteristics of low electronic conductivity, high mechanical strength, high interfacial energy with lithium, and stable chemical properties. It can effectively passivate the surface of lithium metal and inhibit lithium dendrites, but the conduction rate of Li⁺ in the bulk phase is low [41]. Li₃N and Li_xN_oy have high ionic conductivity, but narrow band gap and poor electronic insulation, so

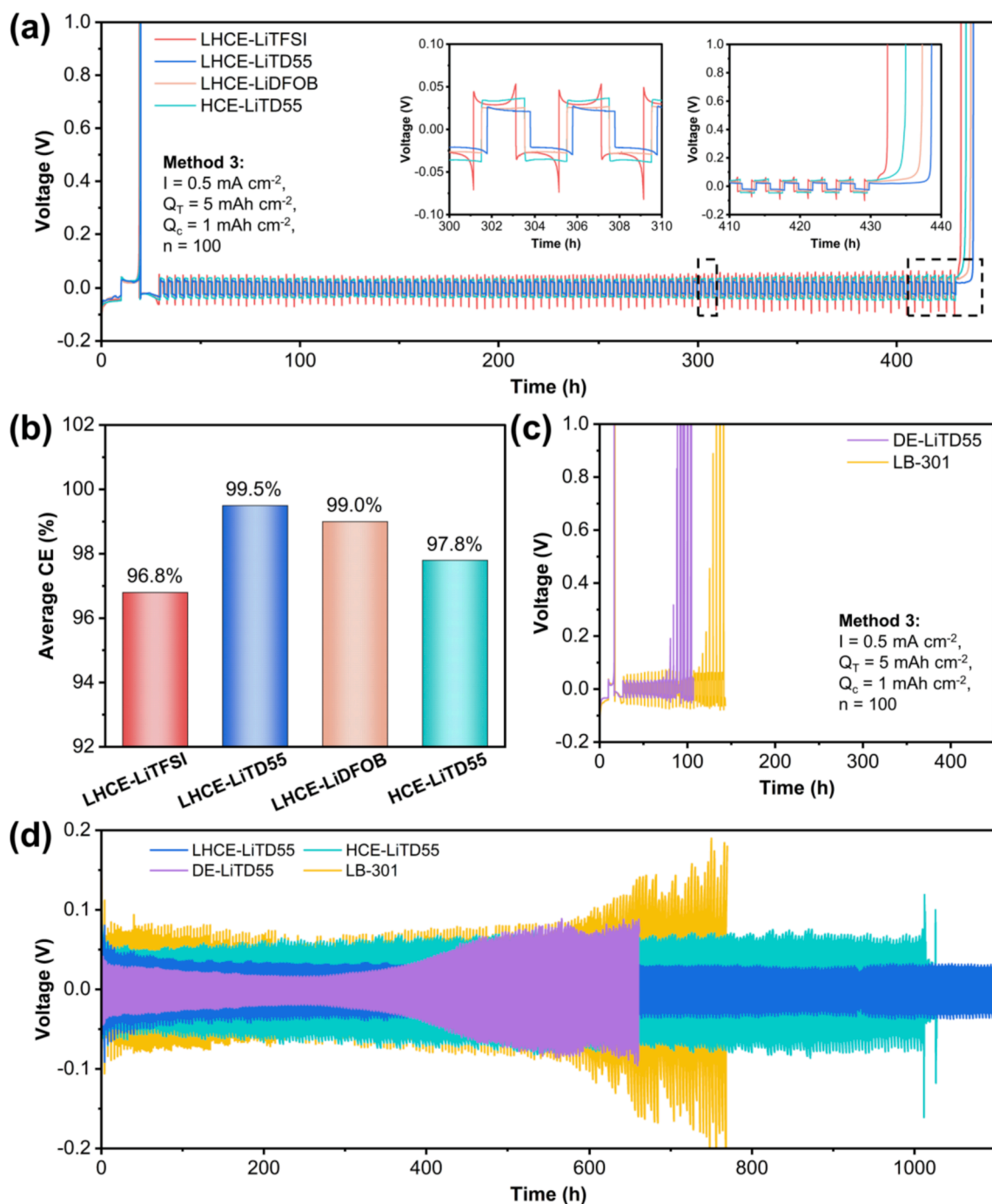


Fig. 2. (a) Average CE tests of Li||Cu cells in different electrolytes (the insets are the voltage profiles of middle and later stages of the CE tests). (b) Comparison of average CEs of Li||Cu cells in different electrolytes. (c) Average CE tests of Li||Cu cells in DE-LiTd55 and LB-301. (d) Cycling performance of Li||Li symmetrical cells using different electrolytes.

they are complementary to LiF in performance [41,42]. In addition, the SEI formed by LHCE-LiDFOB is similar to that of LHCE-LiTd55, but the impedance is larger (Fig. S10) because it does not contain high ionic conductivity components such as Li_3N and Li_xNO_y . Therefore, LHCE-LiTd55 induces the formation of SEI rich in F, N, and B species on the surface of LMA, which can rapidly conduct Li^+ and effectively protect LMA.

Further, the SEI formed from LHCE-LiTd55 was etched to analyze the composition at different depths (Fig. 3c, Fig. S13). After etching for 120 s (24 nm) and 240 s (48 nm), the peak intensities of Li_2O , LiF, and Li_3N increase, while the content of C species decreased significantly. The result shows that the outer layer of SEI formed by LHCE-LiTd55 is

composed of a mixture of inorganic and organic components, while the inner layer is mainly composed of inorganic components.

It is worth noting that XPS characterization of the components of SEI or the solvation structure does not explain why the reversibility of LMA differs greatly in LHCE-LiTd55 and HCE-LiTd55. It has been reported that a slower SEI formation rate favors the formation of more homogeneous and robust SEI, avoiding the production of excess reduction product [22]. TTE is relatively “inert” to the formation of SEI, and the solvated complexes (CIP, AGG) in LHCE-LiTd55 and HCE-LiTd55 is the main reactant for the formation of SEI. Since the concentration of solvated complexes in LHCE-LiTd55 is lower than in HCE-LiTd55, fewer solvated complexes are in contact with lithium metal anode. Therefore,

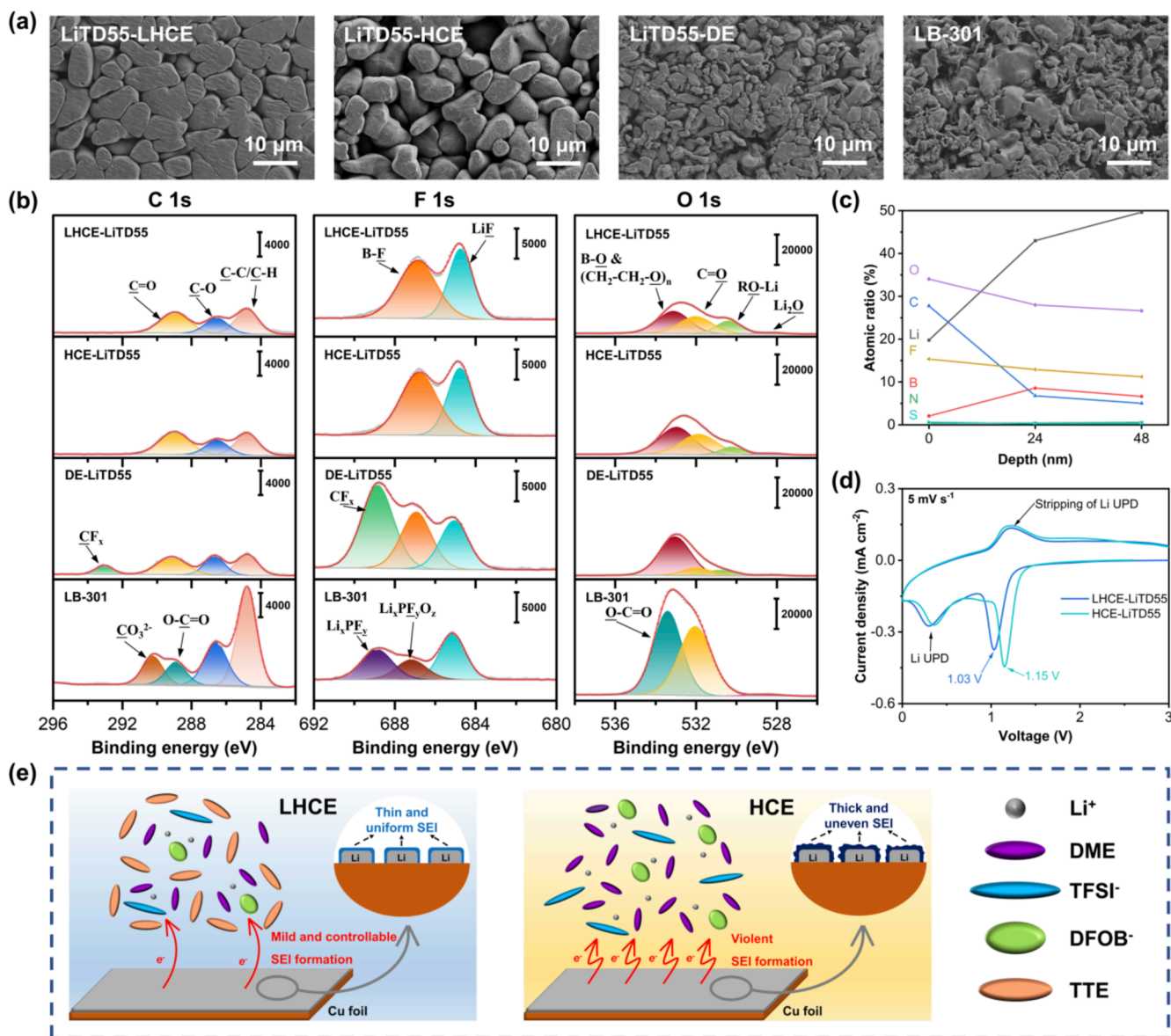


Fig. 3. (a) SEM images of the surface of the deposited lithium in different electrolytes. (b) C 1s, F 1s and O 1s XPS spectra of LMA after cycling in different electrolytes. (c) The XPS atomic ratios of different elements at different depth in SEI formed by LHCE-LiTD55. (d) CV curves of Li||Cu cells in LHCE-LiTD55 and HCE-LiTD55 at a scan rate of 5 mV s⁻¹. (e) Schematic illustration of the process of SEI formation in LHCE-LiTD55 and HCE-LiTD55.

we hypothesize that the role of the diluent TTE is to slow down the rate of SEI formation on LMA by reducing the concentration of solvated complexes (CIP, AGG). To verify the hypothesis, Li||Cu cells with LHCE-LiTD55 and HCE-LiTD55 were subjected to CV tests at different scan rates between 0 and 3 V. At a low scan rate of 0.1 mV s⁻¹, the two reduction peaks around 1.52 V and 0.56 V in the CV curve (Fig. S14a) correspond to the SEI formation and the underpotential deposition of lithium metal (Li UPD), respectively. The reduction potentials and peak intensities of the SEI formation in LHCE-LiTD55 and HCE-LiTD55 are not obviously different, indicating that the reduction reactions occurring in the two electrolytes are almost the same and TTE is hardly decomposed. When the scan rate is increased to 5 mV s⁻¹ (Fig. 3d) and 50 mV s⁻¹ (Fig. S14b), the reduction potential and peak intensity of the SEI formation in HCE-LiTD55 are higher than those in LHCE-LiTD55, indicating that the reduction reaction kinetics of LHCE-LiTD55 are slower than that of HCE-LiTD55. The integral area of the peak of SEI formation in LHCE-LiTD55 is smaller than that in HCE-LiTD55 at high scan rate (Fig. S14c, d), indicating that TTE inhibits the excessive reduction of solvated complexes. It can be concluded that the reduction reaction of

LHCE-LiTD55 is mild and controllable due to the addition of TTE, which promotes the formation of thin and uniform SEI and efficiently improves the reversibility of lithium, as shown in Fig. 3e.

3.3. Compatibility of electrolyte with high-voltage cathode

Li||NCM523 cells were assembled to explore the compatibility of the designed electrolyte with high-voltage cathode. At a charge cut-off voltage of 4.5 V, the cells using LHCE-LiTD55 maintains 90 % capacity retention after 200 cycles (Fig. 4a, b), which can be attributed to the high oxidation stability (oxidative potential > 4.5 V) and the synergistic effect of dual-salt on CEI generation. In contrast, the cells in HCE-LiTD55 and LB-301 showed 82 % and 86 % capacity retention after 200 cycles, respectively, while the cell using DE-LiTD55 suffers from low cycle stability and low CE due to the poor oxidative stability (Fig. 4a, Fig. S15). The SEM (Fig. S16) and XRD (Fig. 4c, Fig. S17) characterization results of the NCM523 cathode after 200 cycles in LHCE-LiTD55 show that its structure is not seriously damaged, which is consistent with the cycle performance.

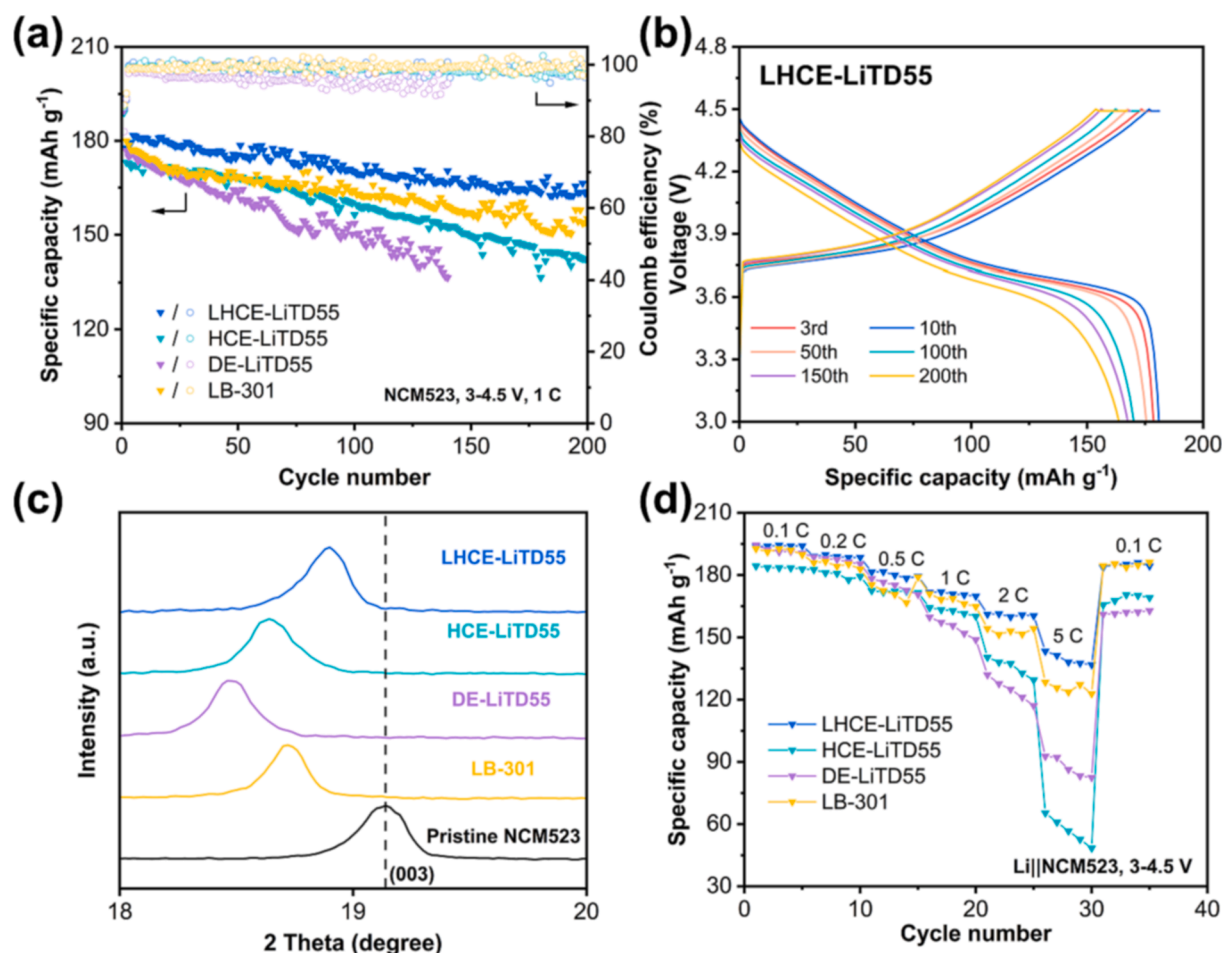


Fig. 4. (a) Cycling performance of Li||NCM523 cells in different electrolytes at a charge cut-off voltage of 4.5 V. (b) The charge–discharge curves of Li||NCM523 cells in LHCE-LiTD55 at a charge cut-off voltage of 4.5 V. (c) XRD characterization results of NCM523 before and after 200 cycles at a charge cut-off voltage of 4.5 V in different electrolytes. (d) Rate performance of Li||NCM523 cells in different electrolytes at a charge cut-off voltage of 4.5 V.

On the other hand, the rate performance of Li||NCM523 cells in different electrolytes was also investigated (Fig. 4d, Fig. S18b, Fig. S19, Fig. S20). The cells in LHCE-LiTD55 exhibit excellent fast-dynamic performance, providing 79 % and 74 % of specific discharge capacity at a rate of 5 C at charge cut-off voltages of 4.3 V and 4.5 V, respectively.

To investigate the mechanism of the electrolyte on the high-voltage cathode, TEM was performed on the cycled NCM523. Firstly, it can be seen from the results of TEM test that CEI exists on the surface of the cathode material that has been cycled in all electrolytes (Fig. 5a, Fig. S21). A uniform layer of CEI with a thickness of about 4 nm is grown in LHCE-LiTD55. The CEI film in LHCE-LiDFOB is thicker than that in LHCE-LiTD55, while in LHCE-LiTFSI, the CEI film is thin but incompletely covered (Fig. S21). This indicates that LiDFOB with good film-forming property can effectively protect the cathode material from corrosion. The CEI film in HCE-LiTD55 is not as uniform as that in LHCE-LiTD55, probably because TTE also participates in the formation of CEI. In DE-LiTD55, the CEI film is thick and non-uniform due to severe decomposition side reactions under high voltage. As for the LB-301, the CEI film is thin but uneven. XPS tests were further performed to detect of CEI components. (Fig. 5b, Fig. S22). The CEI formed by LHCE-LiTD55 is enriched in LiF, B-O, Li_xNO_y , which indicates that LiTFSI and LiDFOB are involved in the generation of CEI. The above-mentioned decomposition products of the lithium salts are considered to be excellent interfacial film components. Combined with the experimental results of TEM on the thickness of CEI, it can be concluded that LHCE-LiTD55 facilitates the growth of a thin and uniform CEI film on the surface of the high-voltage cathode, which has the effect of rapidly conducting Li^+ and

protecting the cathode material.

3.4. Cycling performance of high-voltage lithium metal full-cells

To obtain LMBs with higher energy density, it is necessary to reduce the negative/positive capacity ratio (N/P), which means that there is less excess lithium at the anode, thus aggravating the decrease in cycle stability. NCM523 with high-loading (13 mg cm^{-2}) as cathode and Li@Cu as anode were prepared to assemble lithium metal full-cells. Li@Cu was obtained by electroplating lithium with the same capacity as the positive electrode onto Cu foil and then disassembled it from the Li||Cu cell. Due to the inevitable damage to Li@Cu during the disassembly-reassembly process, the actual N/P is only about 0.9 according to the test (Fig. S23a).

Compared with other electrolytes, Li||NCM523 full-cell using LHCE-LiTD55 exhibits the best cycling stability and highest CE, which is consistent with the results of Li metal reversibility and high-voltage cathode compatibility. At a cut-off voltage of 4.5 V (Fig. 6), the full-cells in LHCE-LiTD55 achieved 70 % capacity retention after 175 cycles with an average CE of 99.5 %, significantly better than those in other electrolytes. For comparison, the cell using HCE-LiTD55 retains only 50 % of its capacity after 108 cycles. Whereas the capacity retention of the cells cycled in DE-LiTD55 and LB-301 rapidly drop below 50 % within 25 cycles due to the poor reversibility of LMA.

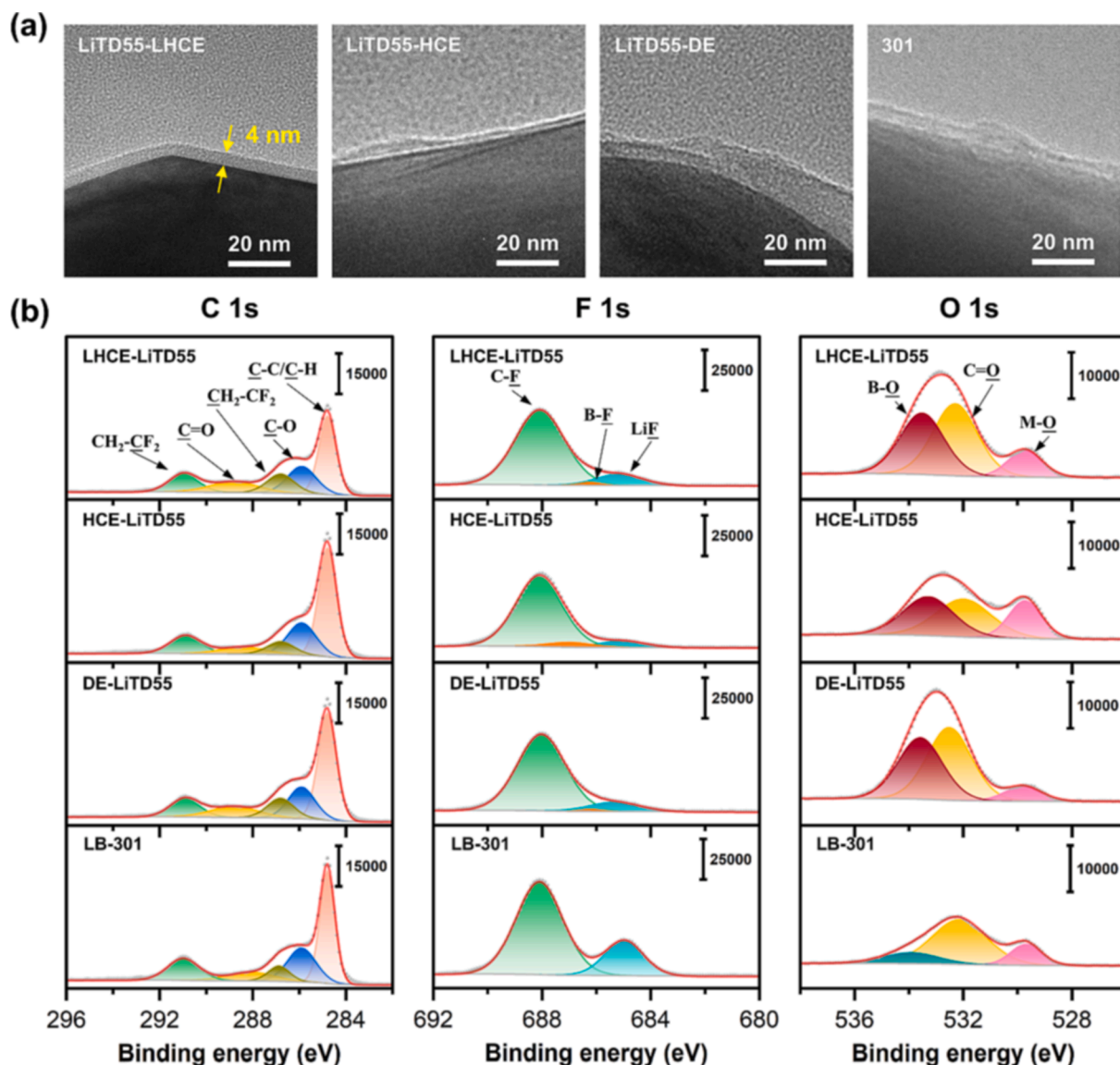


Fig. 5. (a) TEM images and (b) C 1s, F1s and O1s XPS spectra of NCM523 after 10 cycles in different electrolytes.

3.5. Electrochemical performance in a wide-temperature range

The ionic conductivity of different dual-salt electrolytes and LB-301 was tested in a wide-temperature range (Fig. 7a). Benefiting from the low freezing points of TTE and DME, LHCE-LiTD55 remains liquid at extremely low temperature of $-70\text{ }^{\circ}\text{C}$ (Fig. S25). The ionic conductivity of LB-301 drops sharply at $-30\text{ }^{\circ}\text{C}$ due to solidification, while the DE-LiTD55 is always higher in the tested temperature range. For LHCE-LiTD55 and HCE-LiTD55 with similar solvation structure, the low-temperature ionic conductivity of LHCE-LiTD55 is significantly higher than that of HCE-LiTD55. The conductivity of LHCE-LiTD55 can reach 0.176 mS cm^{-1} even at the low temperature of $-40\text{ }^{\circ}\text{C}$, which is 50 times higher than that of HCE-LiTD55. This is mainly due to the fact that the low-temperature viscosity of LHCE-LiTD55 is apparently reduced by TTE compared to HCE-LiTD55.

Previous studies have shown that the electrochemical performance of electrolytes at low temperature is determined by the bulk ionic conductivity and the binding energy of Li^+ to the solvent [43,44]. Li||NCM523 cells in different electrolytes charged to 4.5 V was discharged at a rate of 0.1 C at $-40\text{ }^{\circ}\text{C}$ (Fig. 7b). The low-temperature performance of LHCE-LiTD55 is excellent, enabling the Li||NCM523 cell to provide 71 % (136.1 mAh/g) of the room-temperature discharge capacity. In

contrast, the cells using HCE-LiTD55 and LB-301 have almost no discharge capacity to release, which can be attributed to the too low ionic conductivity of these two electrolytes. The cell in DE-LiTD55 provide only 15 % of the room-temperature discharge specific capacity. Considering that the conductivity of DE-LiTD55 at $-40\text{ }^{\circ}\text{C}$ is significantly higher than that of LHCE-LiTD55, the difference in the low-temperature electrochemical performance of the two electrolytes obviously cannot be explained by the conductivity of the electrolytes. According to the results of classical MD simulations, each Li^+ is on average coordinated by fewer DME molecules and more anions (TFSI^- , DFOB^-) in LHCE-LiTD55 than in DE-LiTD55 (Table S6), which leads to lower binding energy (Fig. 7c). Therefore, Li^+ in LHCE-LiTD55 is more easily desolvated during discharge, leading to higher discharge specific capacity and higher average voltage.

On the other hand, the behavior of different electrolytes at high temperature was also investigated. The side reaction at the interface is more severe at high temperature than at room temperature, threatening the cycling stability of the cell [1,45,46]. At $60\text{ }^{\circ}\text{C}$ and a cut-off voltage of 4.3 V (Fig. 7d, Fig. S26), Li||NCM523 cell using LHCE-LiTD55 has the best cycling stability, providing discharge specific capacities of 160.9 and 152.7 mAh/g after 200 and 400 cycles with capacity retentions of 93 % and 88 %, respectively, and its average CE exceeds 99.5 %. The

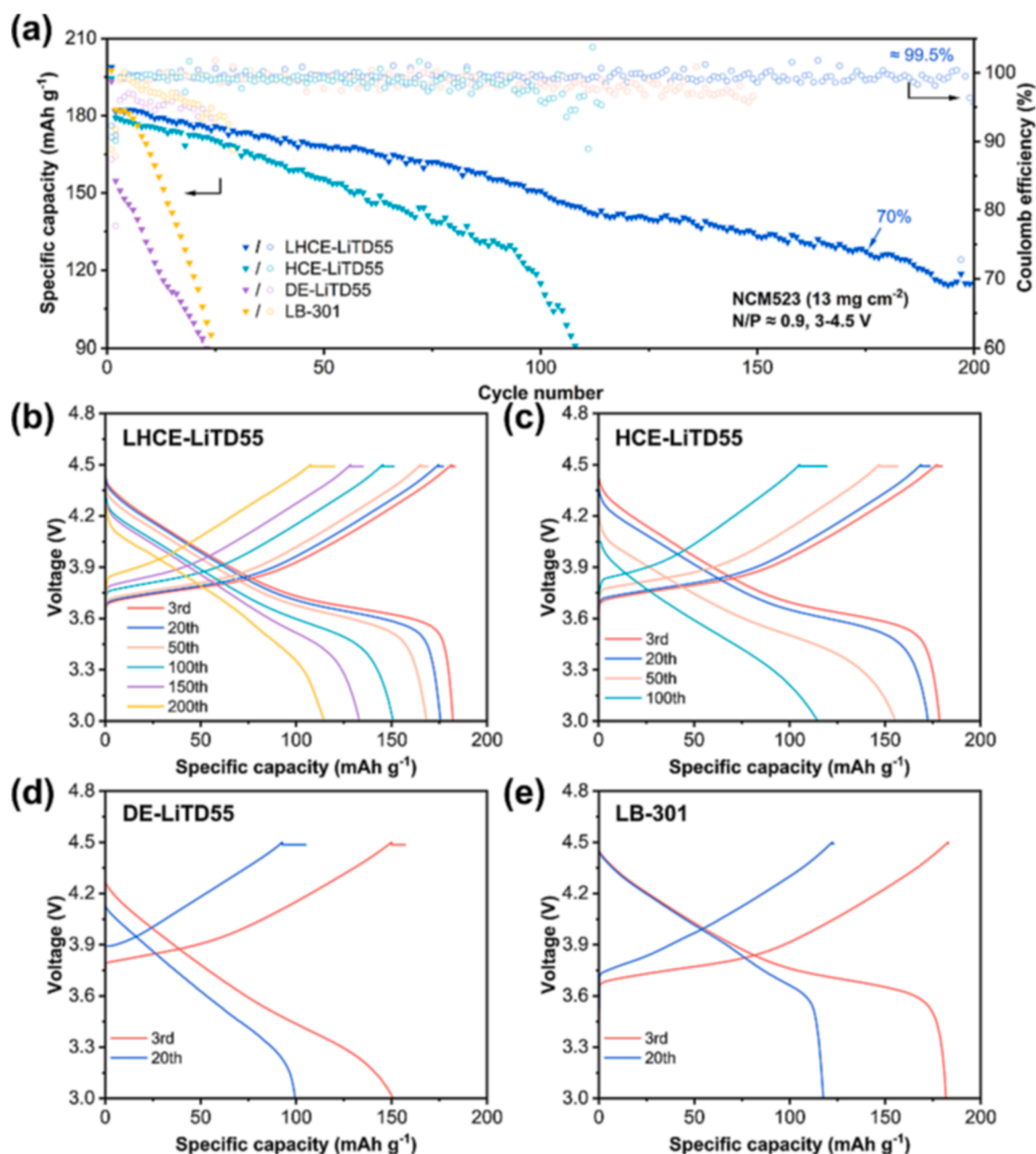


Fig. 6. (a) Cycling performance of Li||NCM523 full-cells in different electrolytes at a charge cut-off voltage of 4.5 V. The charge–discharge curves of Li||NCM523 full-cells in different electrolytes at a charge cut-off voltage of 4.5 V: (b) LHCE-LiTD55, (c) HCE-LiTD55, (d) DE-LiTD55 and (e) LB-301.

cycling stability of the cell in HCE-LiTD55 is close to that in LHCE-LiTD55, but the CE is lower. In contrast, the discharge specific capacity of the cells in DE-LiTD55 and LB-301 decreases rapidly with cycling. Further raising the cycling temperature to 80 °C (Fig. 7e, Fig. S27), the cells in LHCE-LiTD55 exhibited a capacity retention of 85 % (152.2 mAh/g) after 200 cycles and an average CE of about 98.5 %. For comparison, the capacity retention of the cells in HCE-LiTD55 after 200 cycles is 80 %, accompanied by lower CEs, while those in DE-LiTD55 and LB-301 fail within a few cycles due to overcharging. The electrochemical window (4.4 V) of LHCE-LiTD55 measured at 80 °C (Fig. 7f) and the results of DSC test (Fig. S28) also indicated that LHCE-LiTD55 has high thermal stability, which is consistent with the experimental results above.

Based on the above performance of different electrolytes at high temperature, the synergistic effect of the dual-salt and the high ratio of lithium salt to solvent effectively improve the stability of the electrolyte

at high temperature, so that the electrolyte will not be excessively decomposed at the electrode, thus ensuring higher capacity retention and CE. Furthermore, the addition of TTE with lower HOMO energy level also reduces the concentration of free DME molecules and helps to improve the high temperature stability of the electrolyte, which is the reason why the high-temperature performance of LHCE-LiTD55 is better than that of HCE-LiTD55.

4. Conclusion

In this work, a dual-salt ether-based LHCE was designed. NMR, Raman spectra and MD simulations indicate that more anions participate in Li⁺ coordination to form the solvated complexes of CIP and AGG. The synergistic effect of dual-salt and the anion-involved solvation structure play important roles in the formation of the inorganic-rich interfacial layers. The diluent TTE is shown to have little effect on the

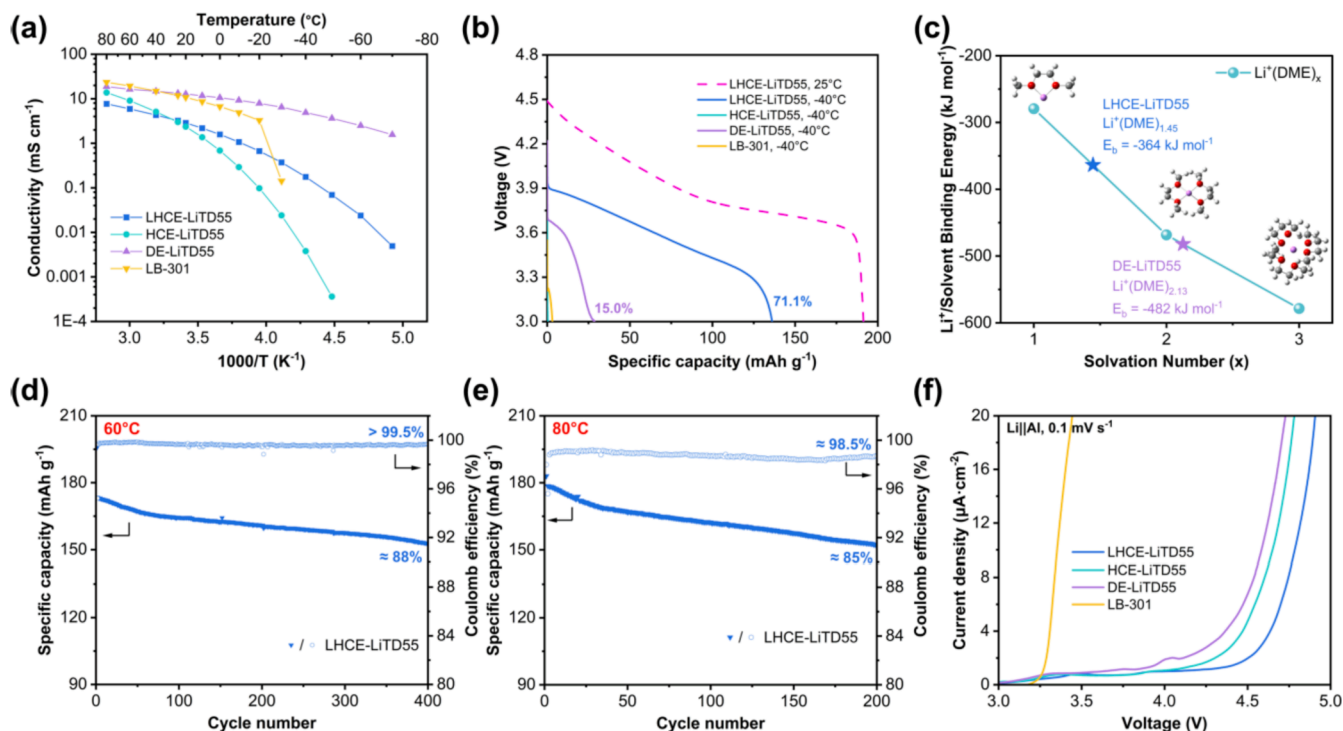


Fig. 7. (a) Measured conductivity of different electrolytes at temperatures from $-70\text{ }^{\circ}\text{C}$ to $80\text{ }^{\circ}\text{C}$. (b) Comparison of discharge curves of Li||NCM523 charged to 4.5 V in different electrolytes at $-40\text{ }^{\circ}\text{C}$. (c) Binding energies of $\text{Li}^+(\text{DME})_{1.45}$ and $\text{Li}^+(\text{DME})_{2.13}$ estimated by linear interpolation (the inset is the optimized structure of $\text{Li}^+(\text{DME})_x$ solvated complex). Cycling performance of Li||NCM523 cells in LHCE-LiTD55 at (d) $60\text{ }^{\circ}\text{C}$ and (e) $80\text{ }^{\circ}\text{C}$, respectively. (f) LSV results at $80\text{ }^{\circ}\text{C}$ of Li||Al cells in different electrolytes at a scan rate of 0.1 mV s^{-1} .

components of SEI, but slows down the reduction of the solvated complex and makes the generation of SEI mild and controllable, effectively improving the reversibility of lithium. As a result, the Li||Cu cell with LHCE-LiTD55 obtains a high average CE of 99.5%. Furthermore, LHCE-LiTD55 shows good oxidative stability due to fewer free DME molecules, the addition of TTE with lower HOMO energy level and the participation of dual-salt in CEI formation at the cathode. Li||NCM523 cell achieves good high-voltage cycling performance at a high cut-off voltage of 4.5 V, with a capacity retention rate of 90% after 200 cycles. To verify the performance in the actual condition, Li||NCM523 full-cell with 0.9 times lithium excess was assembled, which maintains 70% capacity retention after 175 cycles at a cut-off voltage of 4.5 V. In addition, LHCE-LiTD55 also exhibits superior performance in a wide-temperature range. Li||NCM523 cells provide 71% of room-temperature discharge capacity at $-40\text{ }^{\circ}\text{C}$ and retains 88% of capacity after 400 cycles at $60\text{ }^{\circ}\text{C}$. Even raising the temperature to $80\text{ }^{\circ}\text{C}$, Li||NCM523 can be cycled stably for 200 cycles with a capacity retention of 85%. To sum up, this work provides an idea for designing electrolytes suitable for wide-temperature high-voltage LMBs and a new understanding of the role of diluent.

Declaration of Competing Interest

The authors declare that they have no known competing financial interests or personal relationships that could have appeared to influence the work reported in this paper.

Data availability

The authors do not have permission to share data.

Acknowledgments

We gratefully acknowledge the financial support of National Key Research and Development Program of China (2021YFB2400300),

National Natural Science Foundation of China (21875198, 22021001), the key Project of Science and Technology of Xiamen (3502Z20201013) and The Key Research and Development Program of Yunnan Province (202103AA080019). We would like to express gratitude to Tan Kah Kee Innovation Laboratory (IKKEM) for help with XPS, NMR and SEM. And this work was also supported by the High-throughput Computational Platform of Chinese Materials Genome Engineering, which provided high performance computing resources.

Appendix A. Supplementary data

Supplementary data to this article can be found online at <https://doi.org/10.1016/j.cej.2022.139398>.

References

- [1] M.-T.-F. Rodrigues, G. Babu, H. Gullapalli, K. Kalaga, F.N. Sayed, K. Kato, J. Joyner, P.M. Ajayan, A materials perspective on Li-ion batteries at extreme temperatures, *Nat. Energy* 2 (8) (2017) 17108, <https://doi.org/10.1038/energy.2017.108>.
- [2] X. Zhang, L. Zou, Y. Xu, X. Cao, M.H. Engelhard, B.E. Matthews, L. Zhong, H. Wu, H. Jia, X. Ren, P. Gao, Z. Chen, Y. Qin, C. Kompella, B.W. Arey, J. Li, D. Wang, C. Wang, J.-G. Zhang, W. Xu, Advanced Electrolytes for Fast-Charging High-Voltage Lithium-Ion Batteries in Wide-Temperature Range, *Adv. Energy Mater.* 10 (22) (2020) 2000368, <https://doi.org/10.1002/aenm.202000368>.
- [3] D. Luo, M. Li, Y. Zheng, Q. Ma, R. Gao, Z. Zhang, H. Dou, G. Wen, L. Shui, A. Yu, X. Wang, Z. Chen, Electrolyte Design for Lithium Metal Anode-Based Batteries Toward Extreme Temperature Application, *Adv. Sci.* 8 (18) (2021) 2101051, <https://doi.org/10.1002/advs.202101051>.
- [4] Y.-R. Gu, W.-M. Zhao, C.-H. Su, C.-J. Luo, Z.-R. Zhang, X.-J. Xue, Y. Yang, Research Progresses in Improvement for Low Temperature Performance of Lithium-Ion Batteries, *J. Electrochem.* 24 (5) (2018) 488–496, <https://doi.org/10.13208/j.electrochem.180145>.
- [5] V. Kumaravel, J. Bartlett, S.C. Pillai, Solid Electrolytes for High-Temperature Stable Batteries and Supercapacitors, *Adv. Energy Mater.* 11 (3) (2021) 2002869, <https://doi.org/10.1002/aenm.202002869>.
- [6] W. Xu, J.L. Wang, F. Ding, X.L. Chen, E. Nasybutin, Y.H. Zhang, J.G. Zhang, Lithium metal anodes for rechargeable batteries, *Energy Environ. Sci.* 7 (2) (2014) 513–537, <https://doi.org/10.1039/c3ee40795k>.

- [7] D.C. Lin, Y.Y. Liu, Y. Cui, Reviving the lithium metal anode for high-energy batteries, *Nat. Nanotechnol.* 12 (3) (2017) 194–206, <https://doi.org/10.1038/nnano.2017.16>.
- [8] J.-G. Zhang, W.u. Xu, J. Xiao, X. Cao, J. Liu, Lithium Metal Anodes with Nonaqueous Electrolytes, *Chem. Rev.* 120 (24) (2020) 13312–13348.
- [9] N.-W. Li, Y.-X. Yin, J.-Y. Li, C.-H. Zhang, Y.-G. Guo, Passivation of Lithium Metal Anode via Hybrid Ionic Liquid Electrolyte toward Stable Li Plating/Stripping, *Adv. Sci.* 4 (2) (2017) 1600400, <https://doi.org/10.1002/adv.201600400>.
- [10] D. Aurbach, E. Zinigrad, Y. Cohen, H. Teller, A short review of failure mechanisms of lithium metal and lithiated graphite anodes in liquid electrolyte solutions, *Solid State Ion.* 148 (3) (2002) 405–416, [https://doi.org/10.1016/S0167-2738\(02\)00080-2](https://doi.org/10.1016/S0167-2738(02)00080-2).
- [11] E. Peled, S. Menkin, Review—SEI: Past, Present and Future, *J. Electrochem. Soc.* 164(7) (2017) A1703–A1719, <https://doi.org/10.1149/2.1441707jes>.
- [12] F. Ding, W. Xu, X. Chen, J. Zhang, M.H. Engelhard, Y. Zhang, B.R. Johnson, J.V. Crum, T.A. Blake, X. Liu, J.-G. Zhang, Effects of Carbonate Solvents and Lithium Salts on Morphology and Coulombic Efficiency of Lithium Electrode, *J. Electrochem. Soc.* 160(10) (2013) A1894–A1901, <https://doi.org/10.1149/2.100310jes>.
- [13] S. Chen, J. Zheng, D. Mei, K.S. Han, M.H. Engelhard, W. Zhao, W. Xu, J. Liu, J.-G. Zhang, High-Voltage Lithium-Metal Batteries Enabled by Localized High-Concentration Electrolytes, *Adv. Mater.* 30 (21) (2018) 1706102, <https://doi.org/10.1002/adma.201706102>.
- [14] M.S. Park, S.B. Ma, D.J. Lee, D. Im, S.-G. Doo, O. Yamamoto, A Highly Reversible Lithium Metal Anode, *Sci Rep* 4 (1) (2014) 3815, <https://doi.org/10.1038/srep03815>.
- [15] R. Miao, J. Yang, Z. Xu, J. Wang, Y. Nuli, L. Sun, A new ether-based electrolyte for dendrite-free lithium-metal based rechargeable batteries, *Sci. Rep.* 6 (1) (2016) 21771, <https://doi.org/10.1038/srep21771>.
- [16] S.H. Jiao, X.D. Ren, R.G. Cao, M.H. Engelhard, Y.Z. Liu, D.H. Hu, D.H. Mei, J. M. Zheng, W.G. Zhao, Q.Y. Li, N. Liu, B.D. Adams, C. Ma, J. Liu, J.G. Zhang, W. Xu, Stable cycling of high-voltage lithium metal batteries in ether electrolytes, *Nat. Energy* 3 (9) (2018) 739–746, <https://doi.org/10.1038/s41560-018-0199-8>.
- [17] K. Xu, Nonaqueous Liquid Electrolytes for Lithium-Based Rechargeable Batteries, *Chem. Rev.* 104 (10) (2004) 4303–4418, <https://doi.org/10.1021/cr030203g>.
- [18] M. Li, C.S. Wang, Z.W. Chen, K. Xu, J. Lu, New Concepts in Electrolytes, *Chem. Rev.* 120 (14) (2020) 6783–6819, <https://doi.org/10.1021/acs.chemrev.9b00531>.
- [19] J.F. Qian, W.A. Henderson, W. Xu, P. Bhattacharya, M. Engelhard, O. Borodin, J. G. Zhang, High rate and stable cycling of lithium metal anode, *Nat. Commun.* 6 (2015) 9, <https://doi.org/10.1038/ncomms7362>.
- [20] X. Fan, L. Chen, X. Ji, T. Deng, S. Hou, J. Chen, J. Zheng, F. Wang, J. Jiang, K. Xu, C. Wang, Highly Fluorinated Interphases Enable High-Voltage Li-Metal Batteries, *Chem* 4 (1) (2018) 174–185, <https://doi.org/10.1016/j.chempr.2017.10.017>.
- [21] Y. Chen, Z. Yu, P. Rudnicki, H. Gong, Z. Huang, S.C. Kim, J.-C. Lai, X. Kong, J. Qin, Y. Cui, Z. Bao, Steric Effect Tuned Ion Solvation Enabling Stable Cycling of High-Voltage Lithium Metal Battery, *J. Am. Chem. Soc.* 143 (44) (2021) 18703–18713, <https://doi.org/10.1021/jacs.1c09066>.
- [22] J. Alvarado, M.A. Schroeder, T.P. Pollard, X. Wang, J.Z. Lee, M. Zhang, T. Wynn, M. Ding, O. Borodin, Y.S. Meng, K. Xu, Bisalt ether electrolytes: a pathway towards lithium metal batteries with Ni-rich cathodes, *Energy Environ. Sci.* 12 (2) (2019) 780–794, <https://doi.org/10.1039/C8EE02601G>.
- [23] S. Chen, J. Zheng, L. Yu, X. Ren, M.H. Engelhard, C. Niu, H. Lee, W. Xu, J. Xiao, J. Liu, J.-G. Zhang, High-Efficiency Lithium Metal Batteries with Fire-Retardant Electrolytes, *Joule* 2 (8) (2018) 1548–1558, <https://doi.org/10.1016/j.joule.2018.05.002>.
- [24] X.D. Ren, S.R. Chen, H. Lee, D.H. Mei, M.H. Engelhard, S.D. Burton, W.G. Zhao, J. M. Zheng, Q.Y. Li, M.S. Ding, M. Schroeder, J. Alvarado, K. Xu, Y.S. Meng, J. Liu, J. G. Zhang, W. Xu, Localized High-Concentration Sulfone Electrolytes for High-Efficiency Lithium-Metal Batteries, *Chem* 4 (8) (2018) 1877–1892, <https://doi.org/10.1016/j.chempr.2018.05.002>.
- [25] X. Cao, X.D. Ren, L.F. Zou, M.H. Engelhard, W. Huang, H.S. Wang, B.E. Matthews, H. Lee, C.J. Niu, B.W. Arey, Y. Cui, C.M. Wang, J. Xiao, J. Liu, W. Xu, J.G. Zhang, Monolithic solid-electrolyte interphases formed in fluorinated orthoformate-based electrolytes minimize Li depletion and pulverization, *Nat. Energy* 4 (9) (2019) 796–805, <https://doi.org/10.1038/s41560-019-0464-5>.
- [26] S. Li, Q. Liu, W. Zhang, L. Fan, X. Wang, X. Wang, Z. Shen, X. Zang, Y. Zhao, F. Ma, Y. Lu, High-Efficacy and Polymeric Solid-Electrolyte Interphase for Closely Packed Li Electrodeposition, *Adv. Sci.* 8 (6) (2021) 2003240, <https://doi.org/10.1002/adv.202003240>.
- [27] S. Lin, H. Hua, P. Lai, J. Zhao, A Multifunctional Dual-Salt Localized High-Concentration Electrolyte for Fast Dynamic High-Voltage Lithium Battery in Wide Temperature Range, *Adv. Energy Mater.* 11 (36) (2021) 2101775, <https://doi.org/10.1002/aenm.202101775>.
- [28] H. Cheng, Q. Sun, L. Li, Y. Zou, Y. Wang, T. Cai, F. Zhao, G. Liu, Z. Ma, W. Wahyudi, Q. Li, J. Ming, Emerging Era of Electrolyte Solvation Structure and Interfacial Model in Batteries, *ACS Energy Lett.* 7 (1) (2022) 490–513, <https://doi.org/10.1021/acsenergylett.1c02425>.
- [29] S.P. Beltran, X. Cao, J.G. Zhang, P.B. Balbuena, Localized High Concentration Electrolytes for High Voltage Lithium-Metal Batteries: Correlation between the Electrolyte Composition and Its Reductive/Oxidative Stability, *Chem. Mat.* 32 (14) (2020) 5973–5984, <https://doi.org/10.1021/acs.chemmater.0c00987>.
- [30] W. Fan, N.-W. Li, X. Zhang, S. Zhao, R. Cao, Y. Yin, Y. Xing, J. Wang, Y.-G. Guo, C. Li, A Dual-Salt Gel Polymer Electrolyte with 3D Cross-Linked Polymer Network for Dendrite-Free Lithium Metal Batteries, *Adv. Sci.* 5 (9) (2018) 1800559, <https://doi.org/10.1002/adv.201800559>.
- [31] X. Ren, L. Zou, X. Cao, M.H. Engelhard, W. Liu, S.D. Burton, H. Lee, C. Niu, B. E. Matthews, Z. Zhu, C. Wang, B.W. Arey, J. Xiao, J. Liu, J.-G. Zhang, W. Xu, Enabling High-Voltage Lithium-Metal Batteries under Practical Conditions, *Joule* 3 (7) (2019) 1662–1676, <https://doi.org/10.1016/j.joule.2019.05.006>.
- [32] Q.-K. Zhang, X.-Q. Zhang, L.-P. Hou, S.-Y. Sun, Y.-X. Zhan, J.-L. Liang, F.-S. Zhang, X.-N. Feng, B.-Q. Li, J.-Q. Huang, Regulating Solvation Structure in Nonflammable Amide-Based Electrolytes for Long-Cycling and Safe Lithium Metal Batteries, *Adv. Energy Mater.* 12 (24) (2022) 2200139.
- [33] M. Xia, M. Lin, G. Liu, Y. Cheng, T. Jiao, A. Fu, Y. Yang, M. Wang, J. Zheng, Stable cycling and fast charging of high-voltage lithium metal batteries enabled by functional solvation chemistry, *Chem. Eng. J.* 442 (2022), 136351, <https://doi.org/10.1016/j.cej.2022.136351>.
- [34] X. Cao, L. Zou, B.E. Matthews, L. Zhang, X. He, X. Ren, M.H. Engelhard, S. D. Burton, P.Z. El-Khoury, H.-S. Lim, C. Niu, H. Lee, C. Wang, B.W. Arey, C. Wang, J. Xiao, J. Liu, W. Xu, J.-G. Zhang, Optimization of fluorinated orthoformate based electrolytes for practical high-voltage lithium metal batteries, *Energy Storage Mater.* 34 (2021) 76–84, <https://doi.org/10.1016/j.ensm.2020.08.035>.
- [35] B.D. Adams, J. Zheng, X. Ren, W. Xu, J.-G. Zhang, Accurate Determination of Coulombic Efficiency for Lithium Metal Anodes and Lithium Metal Batteries, *Adv. Energy Mater.* 8 (7) (2018) 1702097, <https://doi.org/10.1002/aenm.201702097>.
- [36] F. Qiu, X. Li, H. Deng, D. Wang, X. Mu, P. He, H. Zhou, A Concentrated Ternary-Salts Electrolyte for High Reversible Li Metal Battery with Slight Excess Li, *Adv. Energy Mater.* 9 (6) (2019) 1803372, <https://doi.org/10.1002/aenm.201803372>.
- [37] D. Brouillette, D.E. Irish, N.J. Taylor, G. Perron, M. Odziemkowski, J.E. Desnoyers, Stable solvates in solution of lithium bis(trifluoromethylsulfone)imide in glymes and other aprotic solvents: Phase diagrams, crystallography and Raman spectroscopy, *Phys. Chem. Chem. Phys.* 4 (24) (2002) 6063–6071, <https://doi.org/10.1039/B203776A>.
- [38] J. Fu, X. Ji, J. Chen, L. Chen, X. Fan, D. Mu, C. Wang, Lithium Nitrate Regulated Sulfone Electrolytes for Lithium Metal Batteries, *Angew. Chem.-Int. Edit.* 59 (49) (2020) 22194–22201, <https://doi.org/10.1002/anie.202009575>.
- [39] S.-D. Han, J.L. Allen, E. Jónsson, P. Johansson, D.W. McOwen, P.D. Boyle, W. A. Henderson, Solvate Structures and Computational/Spectroscopic Characterization of Lithium Difluoro(oxalato)borate (LiDFOB) Electrolytes, *J. Phys. Chem. C* 117 (11) (2013) 5521–5531, <https://doi.org/10.1021/jp309102c>.
- [40] P.N. Le Pham, V. Gabaudan, A. Boulaoued, G. Àvall, F. Salles, P. Johansson, L. Monconduit, L. Stievano, Potassium-ion batteries using KFSl/DME electrolytes: Implications of cation solvation on the K⁺-graphite (co-)intercalation mechanism, *Energy Storage Mater.* 45 (2022) 291–300, <https://doi.org/10.1016/j.ensm.2021.11.046>.
- [41] J. Tan, J. Matz, P. Dong, J. Shen, M. Ye, A Growing Appreciation for the Role of LiF in the Solid Electrolyte Interphase, *Adv. Energy Mater.* 11 (16) (2021) 2100046, <https://doi.org/10.1002/aenm.202100046>.
- [42] K. Park, B.-C. Yu, J.B. Goodenough, Li3N as a Cathode Additive for High-Energy-Density Lithium-Ion Batteries, *Adv. Energy Mater.* 6 (10) (2016) 1502534, <https://doi.org/10.1002/aenm.201502534>.
- [43] S.S. Zhang, K. Xu, T.R. Jow, The low temperature performance of Li-ion batteries, *J. Power Sources* 115 (1) (2003) 137–140, [https://doi.org/10.1016/S0378-7753\(02\)00618-3](https://doi.org/10.1016/S0378-7753(02)00618-3).
- [44] J. Holoubek, H. Liu, Z. Wu, Y. Yin, X. Xing, G. Cai, S. Yu, H. Zhou, T.A. Pascal, Z. Chen, P. Liu, Tailoring electrolyte solvation for Li metal batteries cycled at ultra-low temperature, *Nat. Energy* 6 (3) (2021) 303–313, <https://doi.org/10.1038/s41560-021-00783-z>.
- [45] L.-P. Hou, X.-Q. Zhang, B.-Q. Li, Q. Zhang, Cycling a Lithium Metal Anode at 90 °C in a Liquid Electrolyte, *Angew. Chem.-Int. Edit.* 59 (35) (2020) 15109–15113, <https://doi.org/10.1002/anie.202002711>.
- [46] T. Zheng, J. Xiong, X. Shi, B. Zhu, Y.-J. Cheng, H. Zhao, Y. Xia, Cocktail therapy towards high temperature/high voltage lithium metal battery via solvation sheath structure tuning, *Energy Storage Mater.* 38 (2021) 599–608, <https://doi.org/10.1016/j.ensm.2021.04.002>.